Metal Binding Specificity in Carbonic Anhydrase Is Influenced by Conserved Hydrophobic Core Residues†

Jennifer A. Hunt, Mahiuddin Ahmed, and Carol A. Fierke*

Department of Biochemistry, Box 3711, Duke University Medical Center, Durham, North Carolina 27710

Received January 5, 1999; Revised Manuscript Received May 17, 1999

ABSTRACT: The role of highly conserved aromatic residues surrounding the zinc binding site of human carbonic anhydrase II (CAII) in determining the metal ion binding specificity of this enzyme has been examined by mutagenesis. Residues F93, F95, and W97 are located along a β-strand containing two residues that coordinate zinc, H94 and H96, and these aromatic amino acids contribute to the high zinc affinity and slow zinc dissociation rate constant of CAII [Hunt, J. A., and Fierke, C. A. (1997) *J. Biol. Chem. 272*, 20364−20372]. Substitutions of these aromatic amino acids with smaller side chains enhance the copper affinity (up to 100-fold) while decreasing the affinity of both cobalt and zinc, thereby altering the metal binding specificity up to 10^4-fold. Furthermore, the free energy of the stability of native CAII, determined by solvent-induced denaturation, correlates positively with increased hydrophobicity of the amino acids at positions 93, 95, and 97 as well as with cobalt and zinc affinity. Conversely, increased copper affinity correlates with decreased protein stability. Zinc specificity is therefore enhanced by formation of the native enzyme structure. These data suggest that the hydrophobic cluster in CAII is important for orienting the histidine residues to stabilize metals bound with a distorted tetrahedral geometry and to destabilize the trigonal bipyramidal geometry of bound copper. Knowledge of the structural factors that lead to high metal ion specificity will aid in the design of metal ion biosensors and de novo catalytic sites.

Investigating the structural factors that contribute to high metal affinity and specificity in proteins is important in elucidating how naturally occurring metalloproteins recognize and bind specific metal ions. Furthermore, these studies will aid the design and redesign of protein metal binding sites with defined properties. The metal polyhedron in carbonic anhydrase II (CAII)[1] exhibits high zinc affinity and specificity (*1*−*3*), binding only copper and mercury with higher affinity, and has therefore been used as a model for the design of de novo metal binding sites (*4*−*7*). Additionally, the outstanding metal ion selectivity of CAII has been exploited in fluorescence-based biosensors (*8*, *9*) to quantify trace metal ions in complex media for biological, toxicological, and environmental monitoring. Therefore, it is of interest to determine the structural features of CAII that contribute to high zinc affinity and specificity.

The X-ray crystal structure of human CAII (*10*) reveals that the zinc ion is coordinated by histidine residues H94, H96, and H119 at the bottom of a deep active site cleft. At physiological pH, a hydroxide ion is bound to zinc, completing the tetrahedral coordination geometry. High-resolution crystal structures of apo-CAII (*10*) or CAII reconstituted with alternative metals, such as nickel, cobalt, or copper (*11*), reveal very little movement of the coordinating histidines. However, in some cases the geometry of the metal polyhedron is altered due to the recruitment of additional water molecules; the geometry of cobalt-substituted CAII remains tetrahedral, while copper-substituted CAII becomes trigonal bipyramidal. In CAII, the direct zinc ligands form hydrogen bonds with a second shell of residues termed "indirect ligands": the N_δ-H of H94 donates a hydrogen bond to the carboxamide side chain of Q92; the N_δ-H of H96 donates a hydrogen bond to the backbone carbonyl oxygen of N244; the N_ϵ-H of H119 donates a hydrogen bond to the carboxylate side chain of E117; and zinc-bound hydroxide donates a hydrogen bond to the hydroxyl side chain of T199. The effects of altering many of these structural features of CAII have been examined (*1*). Removal of any one of the direct histidine ligands by substitution with alanine reduces the zinc affinity 10^5-fold, while substitution by alternate ligands such as aspartate, asparagine, or glutamate reduces the zinc affinity at least 10^4-fold (*12*, *13*). Alteration of the indirect ligands decreases the zinc affinity 10-fold, while substitutions in E117 greatly increase the zinc equilibration rates (*14*, *15*), possibly by increasing the flexibility of the direct metal ligands. These results suggest that rigid orientation of the direct ligands optimizes zinc affinity and maintains slow zinc dissociation rates.

A further structural feature observed in all metalloproteins is the fact that the hydrophilic direct metal ligands are embedded within a larger shell of hydrophobic groups (*16*).

† Supported by National Institutes of Health (Grant GM40602) and the Office of Naval Research. J.A.H. was partially supported by an NIH Postdoctoral Fellowship (GM17467).

* To whom correspondence should be addressed. Telephone: (919) 684-2557. Fax: (919) 684-8885.

[1] Abbreviations: CAII, human carbonic anhydrase II; EDTA, (ethylenedinitrilo)tetraacetic acid; DPA, dipicolinate; Gdn-HCl, guanidine hydrochloride; MOPS, 3-(*N*-morpholino)propanesulfonic acid; Tris, tris(hydroxymethyl)aminomethane; PAR, 4-(2-pyridylazo)resorcinol; PNPA, *p*-nitrophenyl acetate.

10.1021/bi9900166 CCC: $18.00
Published on Web 06/18/1999

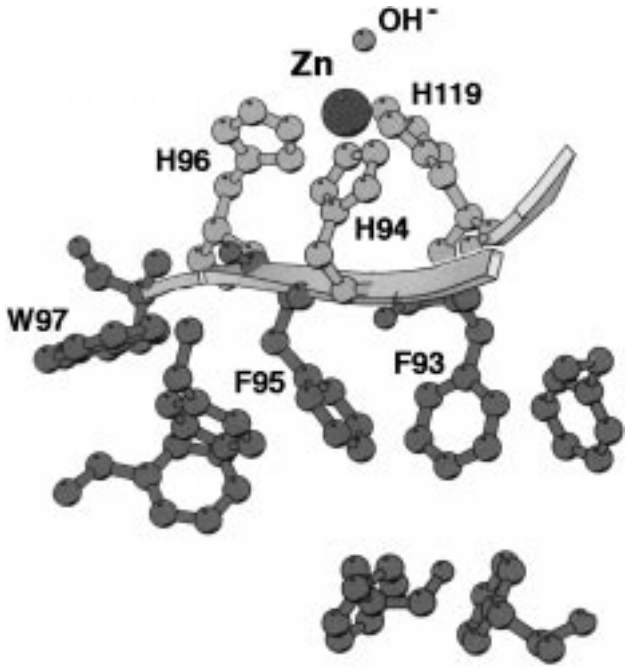

FIGURE 1: Structure of the zinc binding site and hydrophobic cluster of wild-type CAII, taken from the refined crystal structure of Hakansson et al. (*10*), showing the zinc tetrahedrally coordinated to H94, H96, H119, and a solvent molecule and three residues, F93, F95, and W97, that form an aromatic cluster underneath the zinc site. The figure was generated using MOLSCRIPT (*49*).

In CAII, highly conserved residues F93, F95, and W97 flank the zinc ligands H94 and H96 in a β-strand structure (Figure 1) and this aromatic cluster forms packing interactions with the hydrophobic core of the protein, as visualized by X-ray crystallography (*10*). These bulky aromatic residues may increase the affinity of metal binding by restricting the conformational flexibility of the residues coordinating the metal ion and preorganizing the site to enhance zinc binding. Alternatively, the hydrophobicity of these amino acids may be important for providing an interior region with a low dielectric constant to enhance the electrostatic interactions (*16*). Consistent with either of these hypotheses, the zinc affinity of CAII correlates with the size and hydrophobicity of the amino acids at positions 93, 95, and 97; substitution with smaller amino acids reduces the zinc affinity $\leq$100-fold and increases zinc dissociation rate constants up to 1000-fold (*3*).

To delineate these two proposed functions of the conserved aromatic amino acids, we measured the metal specificity and native state stability of six CAII mutants that differ with respect to the size and hydrophobicity of the amino acids substituted at positions 93, 95, and 97. The cobalt affinity of these variants parallels the zinc affinity and decreases as the hydrophobicity of these residues decreases. Surprisingly, the copper affinity shows the opposite trend, increasing as the hydrophobicity decreases so that the Cu^{2+}/Zn^{2+} specificity ratio varies from 50 in wild-type CAII to 9×10^5 in $T_{93}S_{95}V_{97}$ CAII. This differential effect of hydrophobicity of copper and zinc affinity is not consistent with a generalized enhancement of metal coordination due to a low dielectric constant in the protein. Rather, these data suggest that these hydrophobic residues are important for stabilizing a tetrahedral metal ion geometry, as observed for Zn^{2+} and Co^{2+} bound to CAII (*10*), and/or destabilizing alternative geometries, such as the trigonal bipyramidal geometry of Cu^{2+}−CAII (*11*). Consistent with this hypothesis, bound Zn^{2+} or Co^{2+}, but not Cu^{2+}, stabilizes the native state in both wild-type and mutant CAII. Therefore, the high metal specificity and avidity in wild-type CAII are conferred by the well-ordered structure of the native apoenzyme (*10*) which places the histidine ligands in optimal position for forming a tetrahedral metal polyhedron.

MATERIALS AND METHODS

Expression and Purification of CAII Variants. The plasmids encoding CAII variants were originally prepared by cassette mutagenesis (*3*). Two of the mutants ($S_{93}L_{95}M_{97}$ and $T_{93}S_{95}V_{97}$) were isolated directly from this pool. One CAII mutant ($F_{93}I_{95}S_{97}$) was isolated from the pool after one round of selection for CA-phage that bind to sulfonamide resin in the presence of low concentrations of zinc, and the three CAII mutants with the highest zinc affinity ($I_{93}M_{95}V_{97}$, $I_{93}M_{95}W_{97}$, and $F_{93}M_{95}V_{97}$) were isolated after two rounds of selection, as described previously (*3*). These plasmids were transformed into BL21(DE3) cells (*17*), and CAII was induced by the addition of 0.25 mM isopropyl β-D-thiogalactopyranoside to late log *Escherichia coli* BL21(DE3) pACA cells followed by incubation at 30 °C for 5−6 h (*18*). CAII variants were purified using sequential ion exchange chromatography on DEAE-Sephacel and SP-Sepharose Fast Flow, as previously described (*19*).

Metal Dissociation Constants. All solutions were prepared in plasticware using deionized water. Copper and cobalt were obtained from Aldrich as atomic absorption solutions dissolved in nitric acid. To measure the metal dissociation constants, apo-CAII variants were prepared using Amicon diaflow filtration (*20*) against first 50 mM dipicolinate (DPA, pH 7.0) and then 10 mM MOPS buffer (pH 7.0) followed by chromatography on a PD-10 column (Pharmacia) to remove excess DPA. To measure cobalt dissociation constants, apo-CAII (50−80 μM) was dialyzed against varying concentrations of cobalt (0−1 mM) in 0−15 mM citrate and 10 mM MOPS (pH 7.0) for 18−22 h at 30 °C. After equilibrium was achieved, the fraction of CAII containing a bound cobalt ion ([E·Co]) was quantified by measuring the specific PNPA hydrolysis activity (*21*), or by removing free cobalt by chromatography on a PD-10 column and quantifying bound cobalt using a colorimetric 4-(2-pyridylazo)-resorcinol (PAR) assay (*22*). The concentration of free cobalt in the dialysis buffer was calculated from the cobalt−citrate stability constants at 30 °C (*23*). Copper dissociation constants were measured similarly except that apo-CAII was dialyzed against varying concentrations of copper (0−0.33 mM) in 0−2 mM DPA and 10 mM MOPS (pH 7.0). As copper-bound CAII is catalytically inactive, the amount of bound metal was determined using the colorimetric PAR method (*22*). The dissociation constants and standard errors were calculated using the KaleidaGraph curve fitting program (Synergy Software) with eq 1, varying both C and K_{Me}, where C ranged from 0.9 to 1.1.

$$[E\cdot Me]/[E]_{tot} = C/(1 + K_{Me}/[Me]_{free}) \qquad (1)$$

Cobalt Dissociation Rate Constants. The rate constant for cobalt dissociation was determined by preparing apo-CAII variants (40 μM) as described above and reconstituting with 80 μM cobalt sulfate. Co^{2+}-substituted CAII variants (10−

20 μM) were then diluted into 10 mM MOPS (pH 7.0) containing 35 mM EDTA at 25 °C to chelate cobalt dissociating from the enzyme. Since the apoenzyme has low catalytic activity, dissociation of cobalt from CAII was monitored by measuring the decrease in PNPA hydrolysis activity. At various times, aliquots of CAII were diluted 100−200-fold into assay buffer containing 0.1 mM EDTA and the esterase activity was assayed as described above. Data were fit to eq 2 using the curve fitting program KaleidaGraph

$$A_t = A_0 e^{-kt} \quad (2)$$

where A_0 and A_t are the catalytic activity upon addition of EDTA and at various times thereafter, respectively. The standard errors were determined from these fits.

Spectroscopy. Cobalt-substituted enzymes were prepared by adding a 2-fold molar excess of cobalt sulfate to the freshly prepared apoenzyme. Optical absorption spectra were recorded for enzyme solutions (50−100 μM) in 10 mM Tris at pH 9.0 and 25 °C, using a Uvikon double-beam spectrophotometer. Spectra of the Co^{2+} chromophore in Co^{2+}-substituted protein were obtained using a reference cuvette containing the same concentrations of Zn^{2+}−CAII and cobalt sulfate to subtract the contributions from protein absorbance and scattering.

Protein Stability Measurements. The stability of the zinc-bound CAII variants was studied by monitoring guanidine hydrochloride-induced solvent denaturation as previously described (*24*, *25*). CAII variants (0.4−0.8 μM) were incubated in 0.1 M Tris-SO_4 (pH 7.0) containing various concentrations of guanidine HCl (0−2 M) and 1 μM zinc (0.5 μM free zinc) for 18−20 h at 22 °C, and then native CAII was quantified by measuring CO_2 hydration activity (*26*). Increasing the concentration of free zinc to 25 μM did not affect the denaturation profile. The free energy of folding from the intermediate to the native state was calculated at each concentration of guanidine using eq 3

$$\Delta G_{N-I} = -RT \ln(CA^N/CA^I) \quad (3)$$

where CA^N is the percentage of native, or catalytically active CA, and CA^I is the percentage of protein in the intermediate folding state. The free energy in the absence of denaturant ($\Delta G°_{N-I}$) was determined by the linear extrapolation method (*27*) using eq 4.

$$\Delta G_{N-I} = \Delta G°_{N-I} - m_{N-I}[GdHCl] \quad (4)$$

Concentrations of guanidine were confirmed by measuring the index of refraction (*28*).

The stability of copper-bound CAII and cobalt-bound CAII was measured by incubating Cu^{2+}- or Co^{2+}-substituted CAII (10 μM) in 0.1 M MOPS containing various concentrations of guanidine hydrochloride for 18−20 h, and then the percentage of folded protein was quantified by measuring the change in the 292 nm/260 nm absorbance ratio (*29*, *30*). No excess copper was added in these incubations. In cobalt stability determinations, excess cobalt (10−20 μM) was included to ensure that the partially unfolded protein remained bound to cobalt. The stability of apo-CAII was also determined by this method except that 10 μM EDTA was included in the incubated samples to scavenge metal ions. In all cases, eqs 3 and 4 were used to calculate the free energy of folding in the absence of denaturant.

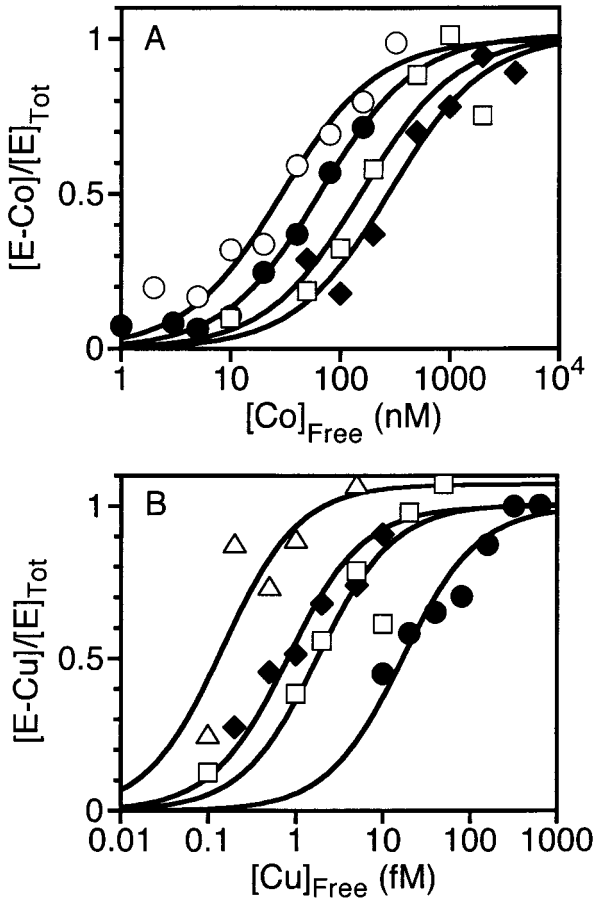

FIGURE 2: (A) Measurement of metal dissociation constants for representative CAII variants. (A) The CAII apoenzyme (0.5 mL of a ≈60 μM solution) was dialyzed for 20 h at 30 °C against 0.5 L of a citrate (0−1 mM)/metal ion buffer (0.2−3 mM cobalt) in 10 mM MOPS buffer (pH 7): $F_{93}M_{95}V_{97}$ (○), $I_{93}M_{95}V_{97}$ (●), $S_{93}L_{95}M_{97}$ (□), and $T_{93}S_{95}V_{97}$ CAII (◆). The amount of enzyme-bound cobalt was calculated from the specific catalytic activity for PNPA hydrolysis. The cobalt dissociation constant was calculated from a fit of these data to eq 1 using the Kaleidagraph curve fitting program. The values of K_{Co} are listed in Table 1. (B) Measurement of copper dissociation constants for representative CAII variants. The CAII apoenzyme was dialyzed for 20 h at 30 °C against 0.5 L of a copper (0−1 mM)/DPA (0.2−3 mM) metal ion buffer in 10 mM MOPS buffer (pH 7): wild-type (●), $S_{93}L_{95}M_{97}$ (□), $F_{93}I_{95}S_{97}$ (◆), and $T_{93}S_{95}V_{97}$ CAII (△). Free copper was removed by gel filtration, and enzyme-bound copper was quantified using the colorimetric PAR assay. The copper dissociation constant was calculated from a fit of these data to eq 1 using the Kaleidagraph curve fitting program. The values of K_{Cu} are listed in Table 1.

RESULTS

Hydrophobic residues F93, F95, and W97 flank the zinc coordinating residues H94 and H96 in a β-strand structure, and participate in packing interactions in a conserved aromatic cluster beneath the zinc binding site (*10*; Figure 1). We have previously demonstrated that the zinc affinity and zinc dissociation rate constant of human CAII correlate with the hydrophobicity of amino acids at positions 93, 95, and 97 (*3*). To distinguish whether this effect is due mainly to the altered dielectric constant of the metal site (*16*) or to preorganization of the tetrahedral metal binding site in the folded protein, we compared the effect of the hydrophobicity

Table 1: Metal Ion Dissociation and Dissociation Rate Constants of CAII Variants

CAII variant	K_{Co}[a] (nM)	Co, k_{off}[b] ($s^{-1} \times 10^6$)	Co, k_{on}[c] (M^{-1} s^{-1})	K_{Cu}[a] (fM)	K_{Zn}[d] (pM)
$F_{93}F_{95}W_{97}$	20 ± 14	5.3 ± 0.4	270	17 ± 4	0.8
$F_{93}F_{95}W_{97}$, denatured[e]	~250			~40	~130
$F_{93}M_{95}V_{97}$	30 ± 10	27± 4	930	3.5 ± 1.1	1.6
$F_{93}I_{95}S_{97}$	240 ± 140	184 ± 6	770	1.4 ± 0.5	6
$I_{93}M_{95}W_{97}$	60 ± 35	14 ± 2	230	5 ± 3	8.0
$I_{93}M_{95}V_{97}$	66 ± 24	30 ± 2	450	3 ± 1	11
$I_{93}M_{95}V_{97}$, denatured[e]				~8	~135
$S_{93}L_{95}M_{97}$	145 ± 100	66 ± 7	450	2 ± 1	29
$S_{93}L_{95}M_{97}$, denatured[e]				~2.5	~220
$T_{93}S_{95}V_{97}$	290 ± 110	90 ± 8	320	0.1 ± 0.1	92

[a] Measured at pH 7.0 and 30 °C. [b] Measured at pH 7.0 and 25 °C. [c] Calculated from $k_{on} = k_{off}/K_{Co}$. [d] Taken from ref *3*. [e] Calculated for the folding "intermediate" using eq 5 with the data in Tables 1 and 2. These values have significant uncertainty due to propagation of errors in K_{Me} and $\Delta G°_{Me,N-I}$.

of these residues on the affinity of two metals that bind to CAII with different geometries, cobalt and copper (*10*, *11*).

Cobalt Affinity of Variants. The cobalt affinities of six CAII variants, containing substitutions at positions F93, F95, and W97 that alter the zinc affinity (*3*), were determined using equilibrium dialysis (Figure 2). The affinity of wild-type CAII for cobalt is 20 nM (Table 1), similar to a previously measured value of 63 nM for CAI (*2*), while the cobalt affinities of all the variants decreased. Substitutions that decrease the overall volume of residues in the hydrophobic cluster by <150 Å^3 decrease the cobalt affinity modestly (1.5−3-fold). The variant containing the smallest and most hydrophilic amino acids at the substituted positions, $T_{93}S_{95}V_{97}$, has the lowest affinity for cobalt (K_{Co} = 290 nM). The cobalt affinities of these variants follow the same trend as their affinities for zinc (*3*), and the free energy for cobalt association [$-RT \ln(1/K_{Co})$] correlates with the hydrophobicity of the amino acids substituted at positions 93, 95, and 97, as indicated by the free energy of transfer between octanol and water (*31*, *32*; Table 1 and Figure 5A).

The X-ray crystal structure of wild-type CAII bound to cobalt reveals that the metal is bound in a tetrahedral geometry, with little alteration in the positions of the coordinating histidines (<0.1 Å) (*11*). To determine whether the variants containing substitutions at residues 93, 95, and 97 also bind cobalt in a tetrahedral geometry, visible absorbance spectra were determined for Co^{2+}-substituted $I_{93}M_{95}V_{97}$, $S_{93}L_{95}M_{97}$, and $F_{93}I_{95}S_{97}$ CAII. Cobalt is a useful probe of metal site structure, as the absorption spectrum of cobalt is sensitive to both the number and nature of the metal ligands (*33*). At pH 9.0, the spectrum of Co^{2+}-substituted wild-type CAII has absorbance peaks at 550 nm (ϵ = 300 M^{-1} cm^{-1}) and 618 nm (ϵ = 320 M^{-1} cm^{-1}) and a secondary peak at 640 nm (ϵ = 250 M^{-1} cm^{-1}) (*34*). The absorbance spectra of the three Co^{2+}-substituted variants at pH 9.0 are virtually identical to the spectrum of wild-type Co^{2+}-substituted CAII (data not shown), suggesting that these variants also bind cobalt in a tetrahedral geometry.

Cobalt Dissociation Rate Constants. To determine whether the decreased cobalt affinity is due mainly to an increased dissociation rate constant, the rate constants for cobalt dissociation were measured for the CAII mutants by dilution into EDTA (Figure 3). As previously observed for zinc (*35*), EDTA does not catalyze cobalt removal but serves to trap free Co^{2+} ions since increasing concentrations of EDTA (10 to 35 mM) do not affect the observed cobalt dissociation rate constant. Cobalt dissociates from wild-type CAII with

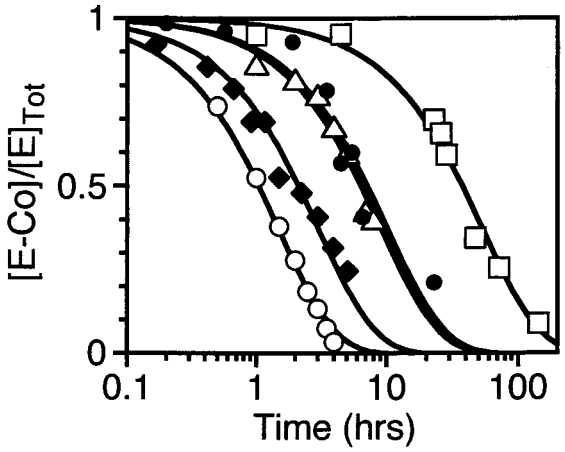

FIGURE 3: Measurement of cobalt dissociation rate constants for CAII variants. Each variant (10−20 μM final concentration), wild-type (□), $F_{93}M_{95}V_{97}$ (●), $I_{93}M_{95}V_{97}$ (△), $T_{93}S_{95}V_{97}$ (◆), and $F_{93}I_{95}S_{97}$ CAII (○), was diluted into 10 mM MOPS buffer (pH 7.0) containing 35 mM EDTA at 25 °C. Dissociation of cobalt was monitored by measuring the PNPA hydrolysis activity of aliquots withdrawn at various times. The cobalt dissociation rate constant was calculated from a fit of these data to eq 2 using the Kaleidagraph curve fitting program. The values of k_{off} are listed in Table 1.

a rate constant of 5.3 × 10^{-6} s^{-1} (Table 1). As the hydrophobicity (*31*, *32*) of the substituted amino acids at positions 93, 95, and 97 decreases, the cobalt dissociation rate constants increase, paralleling the dissociation constant and reaching a maximum of 1.8 × 10^{-4} s^{-1} for the CAII mutant $F_{93}I_{95}S_{97}$.

The association rate constants for cobalt were calculated assuming a simple association reaction where $k_{on} = k_{off}/K_D$ and were found to differ only slightly, ranging from 230 M^{-1} s^{-1} for $I_{93}M_{95}W_{97}$ to 930 M^{-1} s^{-1} for $F_{93}M_{95}V_{97}$ (Table 1). These rate constants are much slower than the association rate constants for zinc [1 × 10^5 M^{-1} s^{-1} (*3*)] and an estimated diffusion-controlled association rate constant (10^8−10^9 M^{-1} s^{-1}) indicating that cobalt binding likely is a multistep process.

Copper Affinity of Variants. To test whether the effects on metal affinity in the CAII mutants are dependent upon the preferred binding geometry of the metal, the dissociation constants for copper were determined for the CAII mutants. Unlike cobalt and zinc, which bind wild-type CAII with a distorted tetrahedral geometry, copper binds to wild-type CAII in trigonal bipyramidal geometry, accepting an additional water as a ligand (*10*, *11*). Using equilibrium dialysis, a K_{Cu} of 17 fM was determined for copper binding to wild-

Scheme 1

$$CA^{N}\text{-}Zn \underset{}{\overset{\Delta G^{\circ}_{N\text{-}I,\,Zn}}{\rightleftharpoons}} CA^{I}\text{-}Zn$$

type CAII (Figure 2B), 50-fold higher than the wild-type CAII affinity for zinc (*3*). Previously, CAI has been demonstrated to bind copper 12-fold more tightly than zinc (*2*). Surprisingly, the copper affinity of all of the mutants is higher than that of wild-type CAII, with dissociation constants ranging from 5.3 fM for $I_{93}M_{95}W_{97}$ to 0.11 fM for $T_{93}S_{95}V_{97}$ CAII (Table 1). As observed for zinc (*3*) and cobalt affinities, copper affinities correlate well with the additive hydrophobicity of the amino acids (*31*, *32*) substituted at positions 93, 95, and 97 except that the affinity increases as the amino acid hydrophobicity decreases (see Figure 5A). The variant $T_{93}S_{95}V_{97}$ CAII binds copper 8×10^5-fold more tightly than zinc, an increase in Cu/Zn specificity of $>10^4$-fold relative to that of wild-type CAII. Therefore, the effect of substitutions in these hydrophobic residues on metal affinity depends on the geometry of the bound metal, indicating that the observed effect is not solely due to changes in the dielectric constant altering electrostatic interactions and suggesting that these aromatic residues are important for stabilizing the tetrahedral metal binding site in the folded protein.

The rate constant for copper dissociation from CAII is not easily determined because copper dissociation is catalyzed by EDTA (0.1−7.6 mM). The dissociation rate constant for wild-type CAII in the absence of EDTA was estimated to be 2×10^{-5} s^{-1} by extrapolating the observed copper dissociation rate constant to 0 M EDTA. If a simple association reaction is assumed, the k_{on} for copper was calculated to occur at the diffusion-controlled rate constant of $\sim 10^9$ M^{-1} s^{-1}.

Stability of Variants. To further investigate the role of these aromatic amino acids in protein stability and metal selectivity, we characterized the solvent-induced denaturation of CAII mutants from the native folded state to the intermediate denatured state at saturating concentrations of zinc ($\Delta G^{\circ}_{N-I,Zn}$, Scheme 1). The equilibrium denaturation of wild-type CAII occurs in two transitions that can be monitored by changes in absorbance (*24*, *25*) reflecting exposure of aromatic residues during unfolding. In the first transition (ΔG_{N-I}), native CAII unfolds to form a thermodynamically stable, partially denatured intermediate "I", which retains much of the secondary structure of the native protein but is catalytically inactive (*25*, *36*, *37*). The second transition (ΔG_{I-U}) reflects further denaturation of this intermediate (*24*, *25*). The first unfolding transition, ΔG_{N-I}, of mutant and wild-type CAII was measured from the decreases in CO_2 hydrase activity following incubation with varying concentrations of guanidine hydrochloride at saturating concentrations of zinc (Figure 4). Monitoring the N−I transition for wild-type CAII via catalytic activity provides results identical to those obtained by monitoring the N−I transition by following changes in absorbance (*24*, *25*) but requires 10−20-fold lower concentrations of protein which minimizes aggregation of the partially unfolded proteins. The I−U transition of these CAII variants was not analyzed since this transition reflects a multiplicity of denatured states (*25*). The free energy of unfolding for the N−I transition of wild-type CAII at pH

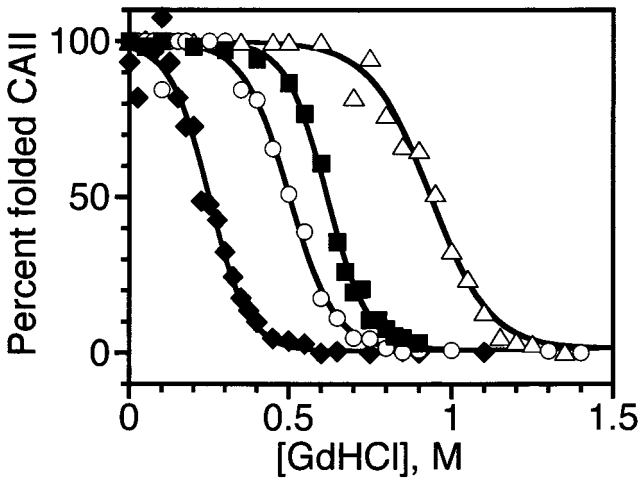

FIGURE 4: Gdn-HCl denaturation of CAII proteins. CO_2 hydrase activity was measured after incubating CAII [wild-type (△), $I_{93}M_{95}V_{97}$ (■), $S_{93}L_{95}M_{97}$ (○), and $T_{93}S_{95}V_{97}$ (◆) CAII] for 18−20 h at 22 °C in 0.1 M Tris-SO_4 (pH 7.0) and 0.5 μM free Zn^{2+} containing 0−1.5 M Gdn-HCl. ΔG°_{N-I} was calculated using eq 4, and the parameters are shown in Table 2.

Table 2: Stability Parameters of Wild-Type and Mutant CAII Proteins

variant	metal	ΔG°_{N-I} (kcal/mol)	m_{N-I} (kcal mol^{-1} M^{-1})	$[GdHCl]_{50}$[a] (M)
$F_{93}F_{95}W_{97}$	Zn^{2+}	7.7 ± 0.5[b]	8.0 ± 0.4	0.96
	none	4.7 ± 0.2[c]	11.3 ± 0.5	0.41
	Cu^{2+}	5.2 ± 0.2[c]	11 ± 0.3	0.46
	Co^{2+}	6.2 ± 0.2[b]	7.4 ± 0.2	0.83
$F_{93}M_{95}V_{97}$	Zn^{2+}	6.8 ± 0.3[b]	7.7 ± 0.4	0.86
$I_{93}M_{95}W_{97}$	Zn^{2+}	7.1 ± 0.7[b]	8.0 ± 0.7	0.88
$I_{93}M_{95}V_{97}$	Zn^{2+}	5.5 ± 0.5[b]	8.8 ± 0.4	0.62
	none	4.0 ± 0.2[c]	9.2 ± 0.4	0.43
	Cu^{2+}	4.5 ± 0.2[c]	9.0 ± 0.3	0.50
$S_{93}L_{95}M_{97}$	Zn^{2+}	3.8 ± 0.2[b]	7.7 ± 0.3	0.50
	none	2.7 ± 0.5[c]	10 ± 1.6	0.26
	Cu^{2+}	2.8 ± 0.3[c]	8.5 ± 1.0	0.33
$T_{93}S_{95}V_{97}$	Zn^{2+}	2.1 ± 0.1[b]	8.6 ± 0.4	0.25

[a] Concentration of guanidine HCl at which CA^N/CA^I is equal to 1. [b] Measured at pH 7.0 and 22 °C by monitoring changes in catalytic activity. [c] Measured at pH 7.0 and 22 °C by monitoring changes in absorbance.

7.0 extrapolated to 0 M guanidine HCl is 7.7 kcal/mol (Figure 4 and Table 2), in good agreement with the previously determined values of 8.4 (*24*) and 7.6 kcal/mol (*25*). The native states of the CAII mutants $F_{93}M_{95}V_{97}$ and $I_{93}M_{95}W_{97}$ are destabilized slightly relative to the intermediate state ($\Delta G^{\circ}_{N-I} = 6.8$ and 7.1 kcal/mol, respectively). However, in the CAII variants $S_{93}L_{95}M_{97}$ and $T_{93}S_{95}V_{97}$, which contain smaller and more hydrophilic amino acids at positions 93, 95, and 97, ΔG°_{N-I} is 4−5 kcal/mol smaller than for wild-type CAII.

The stability of the native state relative to the intermediate state ($\Delta G^{\circ}_{N-I,Zn}$) correlates with the additive hydrophobicity (*31*, *32*) of the substituted amino acids (Figure 5B), with a slope that is near 1 (1.0 ± 0.1). Furthermore, the level of stabilization of the native state relative to the denatured state correlates with increased zinc and cobalt affinity and decreased copper affinity, consistent with the hypothesis that these residues stabilize a tetrahedral metal binding site in the native state compared to the intermediate state.

Stability of Apo- and Metal-Substituted CAII. To further test the role of the aromatic residues in stabilizing a

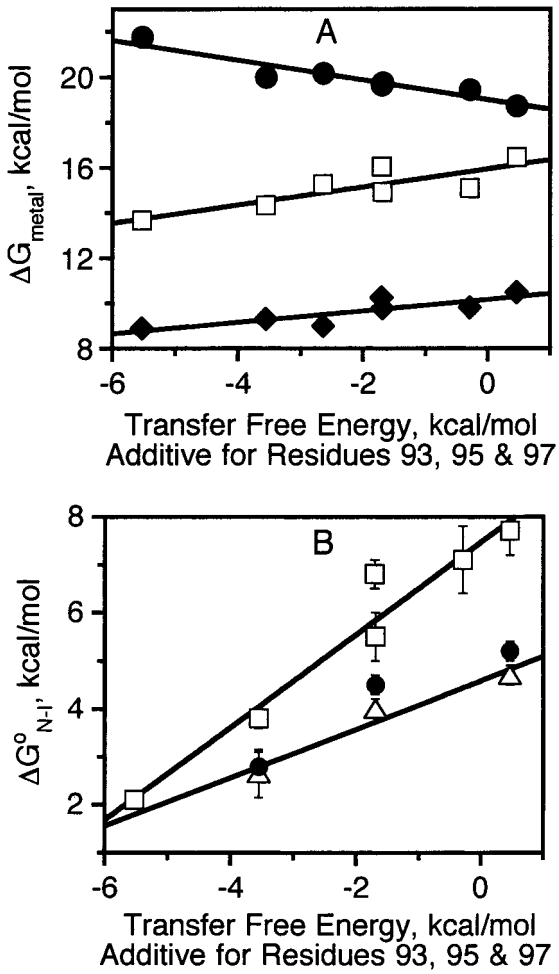

FIGURE 5: (A) Correlation of the free energy for binding cobalt, copper, and zinc to CAII variants with hydrophobicity of residues in the aromatic cluster. The values of ΔG_{Cu} (●) and ΔG_{Co} (◆) (Table 1) and ΔG_{Zn} (□) (taken from ref *3*) for wild-type CAII and CAII proteins varied at positions 93, 95, and 97 are plotted as a function of the additive free energy of transfer of the substituted amino acids between octanol and water (*31*, *32*). The data are fit to a line yielding the following: Cu^{2+}, slope = −0.44 ± 0.07 and $R = 0.94$; Zn^{2+}, slope = 0.4 ± 0.1 and $R = 0.84$; and Co^{2+}, slope = 0.25 ± 0.07 and $R = 0.84$. (B) Correlation of the stability of CAII variants with the hydrophobicity of residues in the aromatic cluster. The values of ΔG°_{N-I} for wild-type CAII and CAII proteins varied at positions 93, 95, and 97 in the absence of metals (△), with bound Zn^{2+} (□) and bound Cu^{2+} (●), are plotted as a function of the additive free energy of transfer of the substituted amino acids between octanol and water (*31*, *32*). The data are fit to a line yielding the following: Zn^{2+}−CAII, slope = 1.0 ± 0.1 and R = 0.97; apo-CAII, slope = 0.5 ± 0.1 and $R = 0.96$; and Cu^{2+}−CAII, slope = 0.6 ± 0.15 and $R = 0.96$.

tetrahedral metal polyhedron, we compared the stability of the apoenzyme and Cu^{2+}-substituted CAII for the wild type and two of the mutants (Table 2). Unfolding was monitored by solvent-induced denaturation in various concentrations of guanidine HCl as indicated by changes in absorbance (A_{292}/A_{260} ratio). These experiments demonstrate that ΔG°_{N-I} for wild-type CAII is dependent on the metal at the active site; ΔG°_{N-I} for zinc-bound, cobalt-bound, and copper-bound CAII is 3, 1.5, and 0.5 kcal/mol, respectively, higher than for apo-CAII (4.7 kcal/mol, Table 2). Interestingly, the slope of the denaturation is steeper for apo-CAII and copper-substituted CAII than for zinc- or cobalt-substituted CAII. In a two-state folding mechanism, the slope of this curve is

Scheme 2

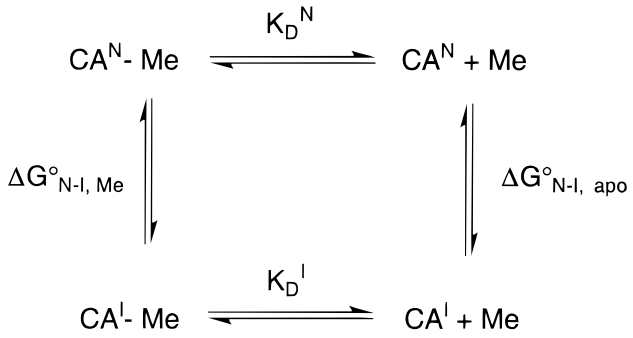

a function of the size and composition of the polypeptide exposed during denaturation (*38*); steeper slopes result from larger changes in the solvent accessible area during unfolding. This suggests that the intermediate might be less compact in the absence of a bound tetrahedral metal.

For the mutant CAII enzymes, bound zinc increases ΔG°_{N-I} compared to that of the apoenzyme by 1.5 and 1.1 kcal/mol for $I_{93}M_{95}V_{97}$ and $S_{93}L_{95}M_{97}$ CAII, respectively (Table 2). This increase in ΔG°_{N-I} is smaller than that observed for wild-type CAII, indicating that the large hydrophobic groups at positions 93, 95, and 97 enhance the stability of the zinc-bound native state relative to the zinc-bound intermediate state (Figure 5B). However, the slight increase in ΔG°_{N-I} for copper-bound CAII compared to that of the apoenzyme (∼0.5 kcal/mol, Table 2) is altered little by changes in the hydrophobicity of amino acids in these positions. Again, these data are consistent with the hypothesis that the hydrophobic shell stabilizes the tetrahedral metal geometry in the native state.

Metal Affinity of the Denatured State. The difference in metal affinity of CAII in the native and intermediate states can be calculated from the increased ΔG°_{N-I} of metal-substituted CAII compared to that of apo-CAII. The free energy differences constitute a closed thermodynamic cycle as shown in Scheme 2 and are represented by eq 5

$$\Delta G^{\circ}_{apo} - RT \ln K_D^N = \Delta G^{\circ}_{Me,N-I} - RT \ln K_D^I \quad (5)$$

where ΔG°_{apo} is the free energy of unfolding of apo-CAII, $\Delta G^{\circ}_{Me,N-I}$ is the free energy of unfolding of metal-bound CAII, K_D^N is the dissociation constant for metal binding to native CAII, and K_D^I is the dissociation constant for metal binding to the partially unfolded intermediate of CAII. When the zinc dissociation constant of 0.8 pM for native Zn−CAII and the free energy of unfolding of both apo-CAII and Zn−CAII are inserted into eq 5, a dissociation constant of ∼100 pM can be calculated for the binding of zinc to the equilibrium folding intermediate of wild-type CAII (Table 2). This affinity is >100-fold lower than that of native CAII. Similarly, the respective cobalt and copper affinities of the denatured intermediate can be estimated to be 0.25 μM and 40 fM, respectively, 12- and 2-fold lower than that of native wild-type CAII, respectively. Therefore, the folding intermediate has decreased binding specificity for zinc compared to that of native CAII. The K_{Zn}/K_{Cu} and K_{Zn}/K_{Co} ratios are changed from 47 and 4×10^{-5}, respectively, for native CAII to 3200 and 5×10^{-4}, respectively, for the folding intermediate. For the proteins with alterations in the hydrophobic shell, the estimated zinc affinity of the denatured

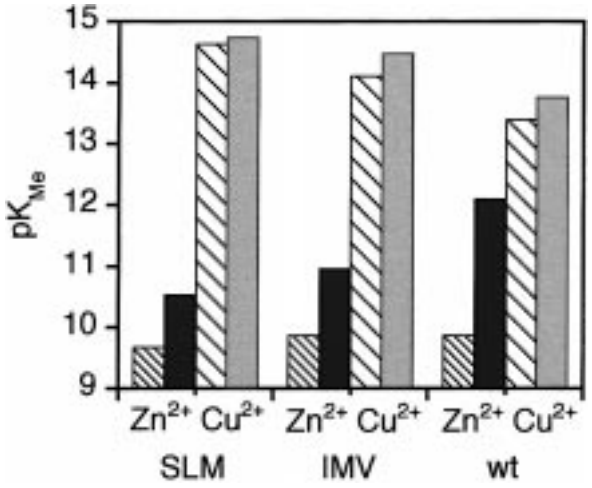

FIGURE 6: Metal dissociation constants ($-\log K_{Me}$) of the native wild type. $I_{93}M_{95}V_{97}$ and $S_{93}L_{95}M_{97}$ CAII (solid bars, Table 1) compared to those of the folding intermediate (hatched bars) calculated using eq 5 with the data in Tables 1 and 2.

intermediate is unchanged (Figure 6) while the copper affinity is enhanced 10-fold. These data suggest that the aromatic residues enhance zinc specificity by both stabilizing a tetrahedral polyhedron in the native state relative to the intermediate denatured state and destabilizing a trigonal bipyramidal geometry in the intermediate and native states relative to other denatured states.

DISCUSSION

Incorporation of the correct metal ion into metalloenzymes in vivo is a crucial step in the biosynthesis of these important enzymes. For some metals, such as copper, transport and metal insertion pathways involve a number of specific proteins (*39*). However, for other metals such as zinc, metal incorporation may be dictated mainly by the metal ion concentration and the thermodynamic and kinetic properties of the metal site. The structural determinants of metal specificity in zinc metalloproteins have not yet been completely elucidated. Among the conserved features near the zinc site of CAII are residues Phe93, Phe95, and Trp97 that lie along the β-strand containing zinc ligands His94 and His96. These residues form packing interactions with other aromatic residues in a conserved hydrophobic cluster beneath the zinc site (*10*) and may serve to make this region of the protein more rigid by decreasing the conformational flexibility of the histidine ligands. Previously, we have demonstrated that residues Phe93, Phe95, and Trp97 are important for high zinc affinity and slow zinc dissociation rate constants (*3*). In this study, we show that these aromatic residues also have an important role in determining the metal binding specificity of CAII and in enhancing protein stability.

Cobalt Affinity. Both cobalt and zinc bind to the metal site of wild-type CAII in a distorted tetrahedral geometry (*10*, *11*); further, the cobalt-substituted enzyme retains 80% of the activity of zinc-CAII. Wild-type CAII binds zinc with high affinity, 16.4 kcal/mol (Table 1), but its affinity for cobalt is significantly lower at 10.5 kcal/mol. This difference in zinc and cobalt affinities is typical of tetrahedral protein zinc sites (*33*) and may be due primarily to the loss of ligand field stabilization energy when cobalt changes from an octahedral coordination in solvent to a tetrahedral coordination in a protein metal site (*40*). Because of its fully occupied d-shell, zinc is not subject to ligand field stabilization effects and incurs little or no energy loss upon changing from octahedral to tetrahedral geometry (*40*).

Substitutions in residues 93, 95, and 97 decrease the affinity of CAII for Co^{2+} (Table 1). As observed for zinc (*3*), the cobalt affinities correlate with both the octanol−water transfer free energy of the amino acids substituted at positions 93, 95, and 97 (Figure 5A) and the protein stability as indicated by $\Delta G^{\circ}_{N-I,Zn}$ (slope $= 0.26 \pm 0.04$; $R = 0.95$). Aromatic amino acids underneath the metal binding site enhance zinc affinity, cobalt affinity, and native state stability. Since zinc and cobalt ions are very similar in size and preferred geometry (*40*, *41*), binding affinities of both metals might be expected to be affected similarly by alterations in the metal binding site. Indeed, spectra of the cobalt-substituted variants indicate that these proteins bind cobalt in a tetrahedral geometry similar to that of wild-type CAII. However, cobalt affinity is decreased less by the substitutions than the zinc affinity; the maximum change in affinity ($\Delta\Delta G$[2]) is 1.6 kcal/mol for cobalt compared to 2.8 kcal/mol for zinc (Table 1). Thus, the Zn/Co specificity (K_{Zn}/K_{Co}) is reduced, from 4×10^{-5} for wild-type CAII to 3×10^{-4} for the $T_{93}S_{95}V_{97}$ mutant. The Zn/Co specificity is similarly reduced (to $\sim 5 \times 10^{-4}$) in denatured CAII (Table 1). Therefore, the conserved aromatic residues in the context of the native protein fold clearly fine-tune the affinity and specificity for zinc so effectively that discrimination between two similar metals, zinc and cobalt (*40*, *41*), is enhanced.

The observed decreases in the cobalt dissociation constants for the CAII mutants with substitutions at positions F93, F95, and W97 can mainly be ascribed to increases in the cobalt dissociation rate constants. As previously observed for Zn^{2+} dissociation (*3*), metal dissociation rate constants increase as smaller and/or more hydrophilic residues are substituted along the β-strand (Table 1). Likely, these substitutions increase the mobility of zinc ligands H94 and H96, facilitating their exchange with solvent. Cobalt association rate constants, with an average of 500 M^{-1} s^{-1} (Table 1), are virtually unaffected by these mutations and are much smaller than the rate constant of zinc association with wild-type CAII at 1×10^5 M^{-1} s^{-1} (*3*). The zinc association rate constant is likely limited by a change in protein conformation since it is significantly enhanced by substitution of (i) smaller amino acids at positions 93, 95, and 97 (*3*) or (ii) E117, a hydrogen bond donor with the direct ligand H119, with D, A, or Q (*14*, *15*). However, the apparent rate constant for cobalt association is insensitive to alterations in the protein structure, suggesting that desolvation may be the rate-limiting step.

Copper Affinities of Mutants. Wild-type CAII binds copper $\sim$50-fold more tightly than zinc, with a copper dissociation constant of 17 fM. This ratio is consistent with the empirically determined Irving−Williams series (*40*), in which small molecule metal chelators commonly exhibit the following preference for metal ions: $Co^{2+} < Ni^{2+} < Cu^{2+} > Zn^{2+}$. All of the mutants examined in this study bind copper more tightly than wild-type CAII; several bind copper as well as naturally occurring copper-binding proteins, which bind copper with K_D values of $\sim$1 fM (*42*). The copper affinities of CAII mutants with alterations in residues 93, 95, and 97

[2] $\Delta\Delta G = -RT \ln(K_{Me}^{Mu}/K_{Me}^{WT})$.

again correlate well with the hydrophobicity of amino acids substituted along the β-strand (Figure 5A) and protein stability as indicated by $\Delta G°_{N-I,Zn}$ (slope $= -0.42 \pm 0.09$; $R = 0.92$). However, this trend is the reverse of that observed for cobalt and zinc affinities; copper affinity is enhanced by substitution of smaller, more hydrophilic residues underneath the metal binding site and by decreasing the native state stability. These data indicate that these aromatic residues both stabilize zinc and destabilize copper binding to the native state, leading to a dramatic increase in the copper specificity (K_{Zn}/K_{Cu}), from 47 for wild-type CAII to 9×10^5 for the $T_{93}S_{95}V_{97}$ mutant. Since zinc and copper ions are very similar in size and preference for coordinating ligand (*40*, *41*), the different bound metal ion geometry [distorted tetrahedral vs trigonal bipyramidal (*10*, *11*)] provides a reasonable explanation for the differential effects of substitutions in the aromatic residues on metal affinity.

Protein Stability. Substitutions at F93, F95, and W97, in the hydrophobic core of the protein, also decrease the native state stability (Figure 4 and Table 2). The unfolding of wild-type CAII occurs in two steps (*24*, *25*, *36*, *37*): (i) native CAII, "N", unfolds to form a stable intermediate, "I", that retains much of the secondary structure of the native protein but is inactive; and (ii) at higher guanidine HCl concentrations, this intermediate further denatures to form the "U" state which is not well-defined but does retain some secondary structure. All of the substitutions in the hydrophobic core destabilize the native state relative to the intermediate state. In fact, the native state stability ($\Delta G°_{N-I,Zn}$) of the hydrophobic cluster variants correlates well with both the additive volume ($R = 0.96$) (*43*) and the additive free energy of transfer from octanol to water of the three amino acids (Figure 5B) (*31*, *32*). The slope of this latter plot is 1, indicating a high dependence of $\Delta G°_{N-I,Zn}$ on the hydrophobic nature of these residues. The stability of the native apoenzyme relative to the denatured state, $\Delta G°_{N-I}$, also decreases as the hydrophobicity of the aromatic cluster is decreased, although the slope of this plot is smaller (Figure 5B), indicating that the hydrophobic nature of these residues is less important for stabilizing the native apoenzyme. Furthermore, the stability ($\Delta G°_{N-I,Zn}$) of these variants correlates with the $\Delta\Delta G^2$ for cobalt (slope $= 0.26$; $R = 0.95$), copper (slope $= -0.42$; $R = 0.92$), and zinc binding (slope $= 0.44$; $R = 0.92$). These data suggest that the alterations in native state stability may be the underlying cause of the observed changes in metal affinity and specificity. The decreased stability of the protein may both lessen (i) the energetic cost of adopting different metal coordination geometries and/or metal−ligand distances and (ii) the energetic gain for forming the optimal tetrahedral geometry.

Metals bound to carbonic anhydrase II stabilize the native conformation relative to the unfolding intermediate (Table 2). However, the amount of stabilization is dependent on the metal ion; for the N−I transition, zinc binding stabilizes native CAII by 3 ± 0.7 kcal/mol, the binding of cobalt provides less stabilization (1.7 ± 0.5 kcal/mol), and copper provides the least stabilization (0.5 ± 0.4 kcal/mol). This increased stability is significantly lower than the ΔG for metal binding (10−19 kcal/mol) and does not correlate with the affinity of the metal ion for the native protein. This apparent paradox indicates that the denatured states of carbonic anhydrase bind metals with altered affinity (Table 2); therefore, the increased stability is caused by the enhanced metal affinity of the native state compared to that of the denatured state (Scheme 1). Alterations in the hydrophobicity of the aromatic cluster decrease the stabilization of the native state by bound zinc (Table 1 and Figure 6) but have little effect on the modest stabilization by copper binding. These data implicate the hydrophobic cluster in stabilizing a tetrahedral metal binding site, perhaps by stabilizing the positioning of the histidine ligands and "indirect" protein ligands in the correct tetrahedral geometry in both the holo- and apoenzymes, as observed by X-ray crystallography (*10*).

Adding such conformational rigidity into designed metal sites may increase both the metal affinity and protein stability of these sites which up to now only bind zinc weakly compared to CAII (*6*, *7*). However, the metal must bind preferentially to the native protein for enhanced protein stability to be observed. The relationship between metal-induced protein stabilization and the formation of high-affinity metal sites has been explored recently in the design of Cys_2His_2 zinc binding sites constructed in thioredoxin (*48*).

Metal Specificity of the Folding Intermediate. The metal binding constants of the CAII folding intermediate can be calculated from the linked equilibria of protein folding and metal binding (Scheme 2 and eq 5). The metal affinity of the wild-type CAII folding intermediate is high (Table 1), with the free energy for zinc dissociation decreasing only 3 kcal/mol compared to that of native CAII. This decrease in metal affinity is even smaller for the CAII mutants with alterations in the aromatic cluster. High metal affinity in the intermediate state is consistent with studies which indicate that the intermediate retains much of the secondary structure of native wild-type CAII, although the catalytic activity is significantly reduced (*24*, *25*). A variety of data (*23*, *36*, *37*, *44*) indicate that the central β-sheet structure of the protein is intact, preserving the position of the three histidines that coordinate zinc, while loop structures are disordered. As histidine ligands 94, 96, and 119 are located on β-strands in this central core, it seems likely that zinc remains coordinated by all three histidine ligands in the folding intermediate. The modest decrease in zinc affinity in the intermediate state also suggests coordination by all three histidine residues; mutagenesis experiments have demonstrated that substitution of one His ligand with Ala decreases the metal affinity in the native state 10^5-fold (*12*). The decrease in affinity in the intermediate could be explained by the loss of one or more hydrogen bonds between the "indirect ligands" and the direct ligands, as each hydrogen bond increases the zinc affinity at least 10-fold (*14*). In particular, loss of a hydrogen bond between T199 and zinc-bound hydroxide could explain both the decreased zinc affinity and the decreased catalytic activity of the intermediate, by comparison with the properties of the T199A CAII mutant (*14*, *45*). Furthermore, denaturation studies of mutants at cis Pro202 (*24*) demonstrate that residue 202 likely forms a trans linkage in the wild-type folding intermediate, indicating that the Ser197−Cys206 loop containing T199 is not in the native configuration. Additional decreases in zinc affinity in the folding intermediate may be caused by increased mobility of the aromatic cluster, as observed by circular dichroism studies (*25*), and the zinc ligands H94 and H96.

The copper affinity of the CAII folding intermediate decreases less than 0.5 kcal/mol compared to those of the

wild type and hydrophobic cluster mutant CAIIs (Table 1). Therefore, copper does not significantly stabilize the fully folded protein relative to the intermediate state and substitutions in the hydrophobic cluster must enhance binding to both the intermediate and native states. These data may be explained by differences in the binding geometries of copper and zinc bound to CAII. Binding of copper to CAII induces several structural changes near the metal site, as visualized in the X-ray crystal structure of Cu^{2+}-substituted CAII (*11*), including the following: (i) copper binds to native wild-type CAII in a trigonal bipyramidal geometry, recruiting a second ligand from solvent; (ii) residue T199 moves 0.14 Å to accommodate this second solvent molecule; and (iii) the zinc-bound solvent molecule is shifted by 1.2 Å, although the hydrogen bond between T199 and this solvent molecule is retained. These rearrangements in the Cu^{2+}-bound native enzyme may be energetically unfavorable and not required in the intermediate state if the hydroxyl side chain of T199 does not form a hydrogen bond with metal-bound solvent.

Possible Physiological Implications. Interestingly, while copper binds more tightly than zinc to both native wild-type CAII and to the folding intermediate of CAII, zinc stabilizes the native folded state more than copper does. Since $\Delta G°_{N-I}$ is greater for zinc-bound than for copper-bound CAII, either CAII folds more rapidly in the presence of zinc than in the presence of copper, or fully folded Cu−CAII unfolds faster than Zn−CAII. Earlier data suggest that zinc-bound CAII folds more rapidly than apo-CAII (*46*, *47*). Once folded, CAII loses zinc extraordinarily slowly, with a $t_{1/2}$ of 95 days (*3*), while preliminary data suggest a $t_{1/2}$ for copper loss of approximately 1 day, suggesting that zinc is kinetically trapped by the folding of CAII. This may be a physiologically relevant method used by metalloproteins to recognize and bind specific metal ions.

ACKNOWLEDGMENT

We thank Dr. Terry Oas, Keith McCall, and Dr. Karen Conklin for helpful discussions.

REFERENCES

1. Christianson, D. W., and Fierke, C. A. (1996) *Acc. Chem. Res. 29*, 331−339.
2. Lindskog, S., and Nyman, P. O. (1964) *Biochim. Biophys. Acta 85*, 462−474.
3. Hunt, J. A., and Fierke, C. A. (1997) *J. Biol. Chem. 272*, 20364−20372.
4. Regan, L., and Clarke, N. D. (1990) *Biochemistry 29*, 10878−10883.
5. Pessi, A., Bianchi, E., Crameri, A., Venturini, S., Tramontano, A., and Sollazo, M. (1993) *Nature 362*, 367−369.
6. Muller, H. N., and Skerra, A. (1994) *Biochemistry 33*, 14126−14135.
7. Vita, C., Roumestand, C., Toma, F., and Menez, A. (1995) *Proc. Natl. Acad. Sci. U.S.A. 92*, 6404−6408.
8. Thompson, R. B., Maliwal, B. P., and Fierke, C. A. (1999) *Anal. Biochem. 267*, 185−195.
9. Thompson, R. B., Maliwal, B. P., Feliccia, V. L., Fierke, C. A., and McCall, K. M. (1998) *Anal. Chem. 70*, 1749−1754.
10. Hakansson, K., Carlsson, M., Svensson, L. A., and Liljas, A. (1992) *J. Mol. Biol. 227*, 1192−1204.
11. Hakansson, K., Wehnert, A., and Liljas, A. (1994) *Acta Crystallogr. D50*, 93−100.
12. Kiefer, L. L., and Fierke, C. A. (1994) *Biochemistry 33*, 15233−15240.
13. Lesburg, C. A., Huang, C.-C., Christianson, D. W., and Fierke, C. A. (1997) *Biochemistry 36*, 15780−15791.
14. Kiefer, L. L., Paterno, S. A., and Fierke, C. A. (1995) *J. Am. Chem. Soc. 117*, 6831−6837.
15. Huang, C.-C., Lesburg, C. A., Kiefer, L. L., Fierke, C. A., and Christianson, D. W. (1996) *Biochemistry 35*, 3439−3446.
16. Yamashita, M. M., Wesson, L., Eisenman, G., and Eisenberg, D. (1990) *Proc. Natl. Acad. Sci. U.S.A. 87*, 5648−5652.
17. Studier, F. W., and Moffat, B. A. (1986) *J. Mol. Biol. 189*, 113−130.
18. Nair, S. K., Calderone, T. L., Christianson, D. W., and Fierke, C. A. (1991) *J. Biol. Chem. 266*, 17320−17325.
19. Krebs, J. F., and Fierke, C. A. (1993) *J. Biol. Chem. 268*, 948−954.
20. Alexander, R. S., Kiefer, L. L., Fierke, C. A., and Christianson, D. W. (1993) *Biochemistry 32*, 1510−1518.
21. Armstrong, J. M., Myers, D. V., Verpoorte, J. A., and Edsall, J. T. (1966) *J. Biol. Chem. 241*, 5137−5149.
22. Hunt. J. B., Neece, S. H., Schachman, H. K., and Ginsburg, A. (1984) *J. Biol. Chem. 259*, 14793−14803.
23. Sillen, L. G., and Martell, A. E. (1964) in *Stability Constants of Metal Ion Complexes, Special Publication No. 17*, The Chemical Society, London.
24. Tweedy, N. B., Nair, S. K., Paterno, S. A., Fierke, C. A., and Christianson, D. W. (1993) *Biochemistry 32*, 10944−10949.
25. Martensson, L.-G., Jonsson, B.-H., Freskgard, P.-O., Kilhgren, A., Svensson, M., and Carlsson, U. (1993) *Biochemistry 32*, 224−231.
26. Brion, L. P., Schwartz, J. H., Zavilowitz, B. J., and Schwartz, G. J. (1988) *Anal. Biochem. 175*, 289−297.
27. Pace, C. N. (1986) *Methods Enzymol. 131*, 266−280.
28. Nozaki, Y. (1972) *Methods Enzymol. 26*, 43−50.
29. Donovan, J. W. (1969) *J. Biol. Chem. 244*, 1961−1967.
30. Edsall, J. T., Mehta, S., Myers, D. V., and Armstrong, J. M. (1966) *Biochem. Z. 345*, 9−36.
31. Fauchere, J. L., and Pliska, V. (1983) *Eur. J. Med. Chem. 18*, 369−375.
32. Eisenberg, D., and McLachlan, A. D. (1986) *Nature 319*, 199−203.
33. Maret, W., and Vallee, B. L. (1993) *Methods Enzymol. 226*, 52−71.
34. Bertini, I., Canti, G., Luchinat, C., and Scozzafava, A. (1978) *J. Am. Chem. Soc. 100*, 4873−4877.
35. Kidani, Y., and Hirose, J. (1977) *J. Biochem. 81*, 1383−1391.
36. Martensson, L.-G., Jonasson, P., Freskgard, P.-O., Svensson, M., Carlsson, U., and Jonsson, B.-H. (1995) *Biochemistry 34*, 1011−1021.
37. Svensson, M., Jonasson, P., Frekgard, P.-O., Jonsson, B.-H., Lindgren, M., Martensson, L.-G., Gentile, M., Boren, K., and Carlsson, U. (1995) *Biochemistry 34*, 8606−8620.
38. Greene, R. F., Jr., and Pace, C. N. (1974) *J. Biol. Chem. 249*, 5388−5393.
39. Koch, K. A., Pena, M. M., and Thiele, D. J. (1997) *Chem. Biol. 4*, 549−560.
40. Huheey, J. E. (1983) *Inorganic Chemistry*, Harper and Row, New York.
41. Glusker, J. P. (1991) *Adv. Protein Chem. 42*, 1−76.
42. Lippard, S. J., and Berg, J. M. (1994) in *Principles of Bioinorganic Chemistry*, University Science Books, Mill Valley, CA.
43. Zamyatnin, A. A. (1972) *Prog. Biophys. Mol. Biol. 24*, 107−123.
44. Jonasson, P., Aronsson, G., Carlsson, U., and Jonsson, B.-H. (1997) *Biochemistry 36*, 5142−5148.
45. Krebs, J. F., Ippolito, J. A., Christianson, D. W., and Fierke, C. A. (1993) *J. Biol. Chem. 268*, 27458−27466.
46. Yazgan, A., and Henkens, R. W. (1972) *Biochemistry 11*, 1314−1318.
47. Wong, K.-P., and Hamlin, L. M. (1975) *Arch. Biochem. Biophys. 170*, 12−22.
48. Wisz, M. S., Garrett, C. Z., and Hellinga, H. W. (1998) *Biochemistry 37*, 8269−8277.
49. Kraulis, P. J. (1991) *J. Appl. Crystallogr. 24*, 946−950.

BI9900166